Energy & Environmental Science

PAPER

View Article Online
View Journal | View Issue

Published on 25 February 2014. Downloaded by Stanford University on 19/05/2014 02:23:01.

Cite this: *Energy Environ. Sci.*, 2014, **7**, 1769

Revisiting film theory to consider approaches for enhanced solvent-process design for carbon capture

Jennifer Wilcox,* Panithita Rochana, Abby Kirchofer, Guenther Glatz and Jiajun He

Received 1st January 2014
Accepted 18th February 2014

DOI: 10.1039/c4ee00001c

www.rsc.org/ees

Application of carbon capture at the gigaton-scale necessary for significant reduction in atmospheric CO_2 requires a portfolio of technologies for applications that may span point-source capture to more dilute systems such as CO_2 removal from the atmosphere. We argue that for absorption separation processes there is a strong coupling between the solvent and process properties, which are uniquely dependent upon the starting concentration of CO_2. We revisit Whitman's film theory and consider mass-transfer correlations to determine the most critical solvent and process parameters that influence the flux of CO_2 from the gas to the liquid phase, within which it is ultimately captured. Finally, results of this work indicate, for instance, that increasing the kinetics of a reacting solvent with CO_2 has a greater impact on direct air capture (DAC) systems, than natural gas- or coal-fired power plant emissions. In addition, the solvent kinetics is a more influential parameter than the Henry's law solubility coefficient for DAC systems, while the reverse may be found for more concentrated CO_2 gas mixtures.

Broader context

Application of carbon capture at the gigaton-scale necessary for significant reduction in atmospheric CO_2 requires a portfolio of technologies for applications that may span point-source capture to more dilute systems such as CO_2 removal from the atmosphere. We argue that for absorption separation processes there is a strong coupling between the solvent and process properties, which are uniquely dependent upon the starting concentration of CO_2. In this work we revisit Whitman's film theory and consider mass-transfer correlations to determine the most sensitive solvent and process parameters that influence the flux of CO_2 from the gas to liquid phase, within which it is ultimately captured. Results of this work will provide insight into new designs of materials and processes for CO_2 capture over a variety of applications in order to meet the gigaton CO_2 challenge, which will require significant reductions of CO_2 at this scale.

Introduction

Carbon capture and storage and utilization (CCS and CCU) are commonly considered a significant component of the portfolio of solutions to slowing global warming. According to the Energy Information Agency's (EIA) *Energy Technology Perspective 2012*, progress in CCS is significantly lagging despite the fact that this technology is anticipated to have significant impact.[1] They estimate that CCS could account for up to 20% of carbon dioxide (CO_2) reductions by 2050, but without large-scale CCS demonstrations rapid deployment in the electricity and industry sectors will be limited.

Global CO_2 emissions reached a record high of 31.6 gigatons (Gt) in 2011, according to preliminary estimates from the International Energy Agency (IEA).[2] Table 1 lists 2009 emissions from energy-related activities, totaling 28.8 Gt, with 43% from coal, 37% from oil, and 20% from natural gas. It has been indicated in previous studies that limiting cumulative CO_2 emissions to 1000 Gt over the 2000–2050 time range would lead to a 25% probability of global warming exceeding 2 °C, while a cumulative limit of 1440 Gt CO_2 leads to a 50% probability of warming beyond 2 °C, which could have irreversible effects on our environment.[3,4] Combining known cumulative emissions[5] from 2000–2006 of ~234 Gt with IEA-reported[6] 2007–2009 estimates of ~87 Gt yields 2000–2009 cumulative emissions of ~321 Gt. Using an estimated annual increase in combined coal, petroleum, and natural gas usage of 1.2% reported by BP in their recent statistical review,[7] *BP Energy Outlook 2030*, business-as-usual (BAU) projected cumulative emissions spanning 2000–2050 are ~1791 Gt, as shown in Table 1. In addition, dependence on coal, petroleum, and natural gas was projected to increase annually by 0.3%, 0.9%, and 2.3%, respectively.[7] To prevent 2 °C warming by 2050 requires avoidance of ~800 Gt of cumulative CO_2 emissions by this time. Although CCS may be only one of the several key components of the portfolio of mitigation strategies,[8–10] several scenarios shown in Table 1 provide insight into the potential impact CCS could have, provided technology is advanced to make this strategy more economically feasible.

Replacing coal with natural gas for electricity generation has the potential to mitigate nearly ~280 Gt CO_2, but alone does not

Department of Energy Resources Engineering, Stanford University, 367 Panama St, Stanford, CA 94305, USA. E-mail: wilcoxj@stanford.edu

Published on 25 February 2014. Downloaded by Stanford University on 19/05/2014 02:23:01.

Table 1 CO_2 mitigation potential of various strategies (in units of Gt)

	2009 emissions	Projected BAU 2050 emissions	Cumulative BAU emissions up to 2050
Coal	12	14	1791
Natural gas	6	15	
Oil	11	15	
Total	29	44	

Scenario	Projected 2050 emissions	Cumulative emissions up to 2050
Coal replaced with natural gas[a]	37	1512
90% capture from electricity sector[b]	28	1251
90% capture from electricity + transportation sectors	22	1025
50% capture from transportation sector[c]	39	1622
50% capture from transportation + 90% capture from electricity	23	1083

[a] Assuming that CO_2 emissions from natural gas are 50% of that from coal, note that this is equivalent to 50% CO_2 capture. [b] Assuming that the fraction of CO_2 generated from the electricity sector is 40%. [c] Assuming that the fraction of CO_2 generated from the transportation sector (road only) is 16%.

bring cumulative emissions near the 1000 Gt target over the 2000–2050 timeframe. Depending on the rank of coal, emissions may range between 835 and 940 g CO_2 per kW per h, while natural gas emits on average 500 g CO_2 per kW per h.[6] Therefore, replacing coal with natural gas is equivalent to ~50% capture of CO_2 from coal-fired units. It is also important to note that the concentration of CO_2 is significantly lower in flue gas of a natural gas-fired unit (*i.e.*, 4–6 mol%) than a coal-fired unit (*i.e.*, 12–14 mol%), which makes CO_2 capture potentially more energy-intensive in the case of natural gas and slightly offsets the 50% reduction in CO_2 emissions.[11,12]

In 2009, emissions associated with the transportation sector constituted ~23% of global emissions, with road transport accounting for ~17%, specifically. Since CO_2 emitted from transportation leads to distributed emissions, the most feasible carbon capture strategy to mitigate transportation emissions would be direct air capture (DAC). However, CO_2 in air is significantly more dilute than CO_2 in the flue gas of a natural gas-fired power plant, with tropospheric CO_2 levels currently estimated at ~400 ppm.[13] A possible alternative is to consider electrifying the transportation sector, allowing for point-source CO_2 capture, which is significantly less energy-intensive and potentially less costly per mole of CO_2 captured. However, it is important to recognize the extensive infrastructure costs that would be required to electrify ground transportation. Another option for possible mitigation of CO_2 from the transportation sector is to replace the current fleet of automobiles (*i.e.*, approximately 1 billion) that run on traditional internal combustion engines burning gasoline and diesel with those that burn hydrogen, resulting in the sole combustion byproduct of water vapor. This of course would require hydrogen, which is primarily sourced from natural gas.[14,15] Hence, alternative strategies would have to be realized to limit CO_2 from H_2 production. This could include advances in electro- and photocatalysis using non-carbonized energy resources such as wind and solar. Another option may be to produce H_2 from natural gas in a process that includes CO_2 capture such as a metallic membrane reactor combined with steam methane reforming and water–gas shift.[16]

It has been well documented that the cost of CO_2 capture from point sources is less expensive than capture directly from the atmosphere;[11,17] however, given the scenarios considered in Table 1, both strategies may be required to prevent 2 °C of warming by 2050. Based upon existing gas separation technologies, the cost of CO_2 capture directly from a coal-fired flue gas has been estimated between \$80–\$100 per ton of CO_2 avoided, while estimates of DAC are reported between \$600–\$1000 per ton of CO_2 avoided.[11,17] The scale of CO_2 to be separated is greater than any gas separation process carried out to date, and due to this scale of CO_2, unless technological advances are made to decrease the costs of capture, this strategy may not play a significant role in preventing global warming. Decreasing these costs will require advances in both material science and process design.

In the current work we show for absorption-based separation processes that there are both process- and material-specific properties that may be ideal for point-source capture *versus* DAC, and that these may be unique to a given application. As technological advances are made in the field of carbon capture, it is important to keep in mind the physical limitations of material-process combinations for a given application. This study focuses on the fundamental separation principles of CO_2 from dilute gas mixtures, including air and the flue gases of natural gas- and coal-fired power plants. In particular, the aim is to provide a deeper understanding of the underlying mechanisms of CO_2 transport from the gas to the liquid phase toward optimization of both process-scale parameters and physical and chemical solvent properties for enhancing mass transfer for each application.

The rate of mass transfer of CO_2 from the gas phase into a captured form is the bridge between the material and the process. In this work, absorption-based processes for CO_2 separation are considered since this approach is more advanced than other separation approaches, such as adsorption or membranes for CO_2 capture at scale. To understand the relationship between material and process properties and their relationship to mass transfer, the two-film model is revisited. First developed by Walter Gordon Whitman in 1923, the two-film model describes the rate of mass transfer within the liquid film at the gas–liquid interface.[18] Focus on this model leads to determining the parameters that are most important to enhancement of mass transfer across the gas–liquid boundary. An increase in mass transfer across this interface may lead to process-scale improvements that will inevitably reduce the costs of separation. For instance, enhanced mass transfer can lead to a reduction in the liquid flow rate in the tower, which will subsequently lead to cost savings in terms of liquid holdup and solvent pumping requirements. Also, a reduction in packing height is possible, which will lead to a decreased pressure drop

 This journal is © The Royal Society of Chemistry 2014

Published on 25 February 2014. Downloaded by Stanford University on 19/05/2014 02:23:01.

and associated costs with gas blowing. Furthermore, a shorter tower results in less packing material, thereby reducing the capital expenses associated with the separation process.

Revisiting Whitman's film theory and the associated assumptions can provide insight as to which thermo-physical or physical-kinetic parameters can most influence the rate of interphase mass transfer for sorption-based CO_2 capture processes. Results of the current work reveal that flue gas and air have properties that make optimal material and process parameters unique for each application, leading to research directions that may be application-specific.

Methodology

In an absorption process for CO_2 separation from a gas mixture, a liquid-phase solvent is pumped downward in an absorption column countercurrent to an upward blown gas mixture containing CO_2. The column is filled with packing material with intrinsic physical properties that maximize gas–liquid contact and minimize the pressure drop through the height of the column. As the solvent passes down the column, it coats the packing material with a thin film that allows for mass transfer of CO_2 from the gas to the liquid phase, with the solvent becoming more enriched with CO_2 as it flows down the column, while the gas mixture becomes increasingly lean in CO_2 as it moves up the column. It follows simply that the degree of CO_2 separation from the gas mixture increases with increasing column height. However, an increase in column height also increases the pressure drop and the capital equipment required for a desired separation.

According to two-film theory, the mass transfer of CO_2 from a gas mixture to a given solvent can be described using a simple model of gas- and liquid-phase films on either side of the gas–liquid interface. Understanding the physical limits of the parameters that dictate the rate of mass transfer in an absorption process will allow for the design of new solvents that can approach these limits. Typical absorption processes may involve (a) a liquid flowing over an inclined or vertical surface, potentially in turbulent flow similar to that of a wetted-wall column, (b) a gas being blown in the form of bubbles through the liquid, (c) a liquid agitated from stirring with entrained gas bubbles in the liquid, or (d) a liquid sprayed through the gas as drops or jets. Correlations have been developed to determine the physical mass-transfer coefficients associated with each of these separation processes. For many scenarios it holds that the mass-transfer resistance is dominant in the liquid film over the gas film. This can be determined by comparing the mass-transfer coefficients of each phase. The next sections describe how mass-transfer coefficients may be determined from available correlations in the literature and how these coefficients lead to determining the flux of CO_2 across the gas–liquid interface to a captured state.

1 Mass-transfer correlations

The mass-transfer resistances in the gas and liquid films are often considered in series, and can be described by the following relationship:[19–22]

$$\frac{1}{K_G} = \frac{1}{k_G} + \frac{H}{Ek_L} \quad (1)$$

such that K_G is the overall gas-phase mass-transfer coefficient, k_G is the individual gas-phase mass-transfer coefficient, E is the enhancement factor for chemical capture (for purely physical absorption-based processes, E is equal to unity), k_L is the purely physical liquid-phase mass-transfer coefficient, and H is the Henry's law constant defined by:

$$p_{CO_2} = Hc_{CO_2} \quad (2)$$

such that p_{CO_2} is the partial pressure of CO_2 in equilibrium with the liquid phase at the gas–liquid film, and c_{CO_2} is the concentration of CO_2 in the solvent. In eqn (1), K_G and k_G have units of kmol m^{-2} s^{-1} atm, while k_L has units of m s^{-1} (expressed in mm s^{-1} throughout this work), H has units of atm m^3 mol^{-1}, and E is dimensionless. It is crucial that the Henry's law expression is first determined before using eqn (1) since the Henry's law can be written in multiple forms, with another common form being dimensionless if H is divided by RT, where R is the ideal gas constant and T the temperature. The form of Henry's law used in the current work as expressed in eqn (1) and (2) is consistent with traditional chemical engineering convention as presented in Seader,[19] Dankwerts,[21] and McCabe *et al.*[22]

A number of empirical and semi-theoretical mass-transfer models are available in the literature. These models are useful for their prediction of hydrodynamic and mass-transfer phenomena for design and analysis for gas separation using packed columns. Since the current work focuses on a variety of applications, spanning DAC to CO_2 capture from flue gas, it is important to acknowledge the limited data associated with CO_2 capture applications from air. To the authors' knowledge, there have been few cases in which designs for DAC plants have been proposed.[23,24] In the work of Holmes and Keith[23] a design and fabrication of an air-liquid contactor is proposed based upon methods derived from cooling tower technology. Mazzotti *et al.*[24] propose a more traditional design approach based upon a conventional contactor that may be more suited for flue gas applications. The widely used models of Onda *et al.*[25] and Fair and Bravo,[26] which are based upon solvent wetting of random packing material, will be used in the current work to investigate the sensitivity of the solvent physical properties on mass transfer from the gas to the liquid phase. Again, these correlations are based on conventional counter-flow systems, and it should be recognized that if a more rigorous approach were used for solvent-process design, *i.e.*, correlations specific to the cross-flow systems traditionally used for cooling towers, this would provide greater insight for DAC applications.

The *gas-phase* mass-transfer coefficient correlation developed by Fair and Bravo[26] is:

$$k_G = 0.0338\left(\frac{D_{CO_2}}{a_t d_p^2}\right)\left(\frac{\rho G}{a_t \mu}\right)^{0.8}\left(\frac{\mu}{\rho D_{G,CO_2}}\right)^{1/3} \quad (3)$$

such that D_{G,CO_2} is the diffusivity of CO_2 in the gas phase [m^2 s^{-1}], a_t is the specific surface area of packing [m^2 m^{-3}], d_p is the packing diameter [m] defined as $6(1-\varepsilon)/a_t$, where ε is the void

Published on 25 February 2014. Downloaded by Stanford University on 19/05/2014 02:23:01.

fraction of the packing,[27] ρ is the gas density [kg m^{-3}], G is the superficial gas velocity [m s^{-1}], and μ is the gas viscosity [kg m^{-1} s^{-1}]. Although Fair and Bravo[26] suggested that the gas-phase mass-transfer coefficient expression may range between 0.018 and 0.040, previous studies commonly use a coefficient of 0.0338, which is adopted in the current investigation.

The gas-phase mass-transfer coefficient is also commonly written in terms of the Sherwood (Sh), Reynolds (Re) and Schmidt dimensionless numbers (Sc) as:

$$\mathrm{Sh} = k_{\mathrm{G}}\left(\frac{a_{\mathrm{t}}{d_{\mathrm{p}}}^{2}}{D_{\mathrm{CO_2}}}\right) = 0.0338\mathrm{Re}^{0.8}\mathrm{Sc}^{1/3} \quad (4)$$

Mass-transfer correlations are often of the form that involves a Sherwood number containing the mass-transfer coefficient for either the gas or the liquid phase. The Sherwood number varies with the Schmidt number, which is the ratio of diffusivities based upon momentum to mass. In addition, the Sherwood number depends upon the flow field, which is unique to the fluid. For instance, for DAC, the airflow field is dictated by atmospheric conditions such as wind velocity. In the case of a power plant (natural gas or coal), the flow properties are based upon fans or blowers located upstream of the absorption column for CO_2 capture. In the case of the liquid mass-transfer correlation, the solvent flow properties are dictated by pumping or forced convection. The Reynolds number is the ratio of inertial to viscous forces.

The *liquid-phase* mass-transfer coefficient correlation developed by Onda *et al.*[25] is:

$$k_{\mathrm{L}} = 0.0051\left(a_{\mathrm{t}}d_{\mathrm{p}}\right)^{0.4}\left(\frac{\mu g}{\rho}\right)^{1/3}\left(\frac{\rho L}{a_{\mathrm{w}}\mu}\right)^{2/3}\left(\frac{\mu}{\rho D}\right)^{-1/2} \quad (5)$$

such that μ is the liquid viscosity [kg m^{-1} s^{-1}], ρ is the liquid density [kg m^{-3}], g is the gravitational constant [m s^{-2}], L is the superficial liquid velocity [m s^{-1}], D is the diffusivity of CO_2 in the liquid phase [m^2 s^{-1}], and a_{w} is the wetted surface area of the packing material [m^2 m^{-3}]. Onda *et al.*[25] investigated the application of film theory of CO_2 absorption into aqueous solutions of NaOH in packed columns and confirmed that the wetted surface area, a_{w}, is identical to the gas–liquid interface, across which mass transfer of CO_2 takes place. From the work of Onda *et al.*,[28] the correlation between a_{w} and total packing surface area can be expressed as:

$$\frac{a_{\mathrm{w}}}{a_{\mathrm{t}}} = 1 - \exp\left\{-1.45\left(\frac{\sigma_{\mathrm{c}}}{\sigma}\right)^{0.75}\left(\frac{\rho L}{a_{\mathrm{t}}\mu}\right)^{0.1}\left(\frac{L^2 a_{\mathrm{t}}}{g}\right)^{-0.05}\left(\frac{\rho L^2}{\sigma a_{\mathrm{t}}}\right)^{0.2}\right\} \quad (6)$$

such that σ_{c} is the critical surface tension of the packing material and σ is the interfacial tension [N m^{-1}] of the liquid. The critical surface tensions for ceramic- and steel-based random packing materials are 0.061 and 0.075 N m^{-1}, respectively.[29]

k_{L} and a_{w} can also be expressed in terms of dimensionless numbers as follows:

$$k_{\mathrm{L}}\left(\frac{\rho}{\mu g}\right)^{1/3} = 0.0051\left(a_{\mathrm{t}}d_{\mathrm{p}}\right)^{0.4}\mathrm{Re}^{2/3}\mathrm{Sc}^{-1/2} \quad (7)$$

and

$$\frac{a_{\mathrm{w}}}{a_{\mathrm{t}}} = 1 - \exp\left\{-1.45\left(\frac{\sigma_{\mathrm{c}}}{\sigma}\right)^{0.75}\mathrm{Re}^{0.1}\mathrm{Fr}^{-0.05}\mathrm{We}^{0.2}\right\} \quad (8)$$

such that Fr is the Froude number and We is the Weber number. The Froude number is the ratio between the inertial and the gravitational forces, while the Weber number is the ratio between the inertial and the interfacial tension forces acting on a given fluid particle. The expression for a_{w} is valid across the following conditions:

$$0.04 < \mathrm{Re} < 500$$

$$1.2 \times 10^{-8} < \mathrm{We} < 0.27$$

$$2.5 \times 10^{-9} < \mathrm{Fr} < 1.8 \times 10^{-2}$$

$$0.3 < \sigma_{\mathrm{c}}/\sigma < 2.0$$

These correlations allow for the physical gas- and liquid-phase mass-transfer coefficients to be determined, which lies at the heart of designing new solvents with material and physical properties optimized for a given carbon capture application. These correlations, since they are only comprised of physical properties, will not provide information on how the mass-transfer coefficients are enhanced with chemical reaction. The inclusion of chemical enhancement requires introduction of the enhancement factor, which depends upon properties of the chemical reaction taking place between CO_2 and the binding species (*i.e.*, amine, hydroxyl, *etc.*), discussed in detail in the next section.

2 Liquid-phase resistance and film models

In general, the presence of a chemical reaction can significantly influence the mass transfer of CO_2 into the liquid phase. The enhancement factor, E, is the ratio of the average rate of absorption into an agitated liquid in the presence of a reaction to the average rate of absorption without the enhancing reaction. If dissolved CO_2 gas reacts with a dissolved binding material, B, by an irreversible second-order reaction, $CO_2 + zB \xrightarrow{k} P$, the rate of CO_2 absorption into the solution with a reaction is influenced by a number of factors, including CO_2 solubility, mass transfer, diffusivity, reaction kinetics, *etc.* The stoichiometric coefficient, z, of the reactive binding species B, is also an important parameter included in the absorption calculation. If the molar ratio between CO_2 and the binding species in a given reaction is 1 : 2, then $z = 2$. The balanced chemical reaction must be written out in order to determine z accurately. In general, regardless of the mass-transfer model assumed, the rate of absorption with a reaction is related to the liquid-phase (physical) mass-transfer coefficient, k_{L}, as:

$$J_{\mathrm{L,CO_2}} = c_{\mathrm{i}}k_{\mathrm{L}}E \quad (9)$$

such that E is the enhancement factor that only plays a role in chemically binding solvents. Additionally, if CO_2 reacts fairly closely to the gas–liquid interface, it can be assumed that it reacts

 This journal is © The Royal Society of Chemistry 2014

Published on 25 February 2014. Downloaded by Stanford University on 19/05/2014 02:23:01.

fast and that the concentration of CO_2 distant from the interface (*i.e.*, c_{∞,CO_2}) is approximately zero. In practical applications, this scenario is not necessarily favored since an energy-efficient reversible process requires near-equilibrium conditions.

In the case of the film model, van Krevelen and Hoftijzer[30] computed the approximate solution to the enhancement factor

$$E = \frac{\sqrt{M\left(\frac{E_i - E}{E_i - 1}\right)}}{\tanh\sqrt{M\left(\frac{E_i - E}{E_i - 1}\right)}} \quad (10)$$

such that

$$\sqrt{M} = \frac{\sqrt{Dkc_B}}{k_L} \quad (11)$$

and

$$E_i = \left(1 + \frac{D_B c_B}{z D c_i}\right) \quad (12)$$

such that E_i is the enhancement factor corresponding to an instantaneous reaction, D is the CO_2 diffusivity in the liquid phase, k is the forward rate constant of CO_2 with the binding species, k_L is the liquid-phase mass-transfer coefficient, c_i is the concentration of CO_2 at the gas–liquid interface, and c_B is the bulk concentration of the binding species in solution. For a fixed value of E_i, an increase in $\sqrt{M}$ leads to an increase in E as a limiting value is approached, in which case $E = E_i$. Several criteria associated with $\sqrt{M}$ in the calculation of E will be discussed and are outlined in Table 2. For instance, when $\sqrt{M} > 10E_i$, the enhancement factor is approximately equal to that of an instantaneous reaction. Physically, this is the case when the reaction rate constant is high and the rate of mass transfer is limited by the rate of the diffusion of reaction products away from the gas–liquid interface.

If $\sqrt{M} < 1/2E_i$, the reaction can be considered pseudo-first-order and the enhancement factor can be calculated from $\sqrt{M}/\tanh\sqrt{M}$, as shown in Table 2. This is the case in which the reaction is sufficiently slow, or the physical mass-transfer coefficient is sufficiently large, that the concentration of the CO_2 binding material is nearly undepleted with its bulk concentration, c_B, consistent throughout the depth of the liquid phase to the interface. If this condition holds in addition to $\sqrt{M} > 3$, then to a reasonable approximation,

$$E = \sqrt{Dkc_B} \quad (13)$$

Table 2 Limiting cases of the film model

Limiting case	Enhancement factor	Physical explanation
(1) $\sqrt{M} > 10E_i$	$E = E_i$	Instantaneous reaction
(2) $\sqrt{M} < 1/2\ E_i$	$E = \left(\frac{\sqrt{M}}{\tanh\sqrt{M}}\right)$	Pseudo-first-order reaction
(3) #2 satisfied and $\sqrt{M} > 3$	$E = \sqrt{Dkc_B}$	Fast pseudo-first-order reaction
(4) None of the above	Determine E from Fig. 1 or eqn (10)	

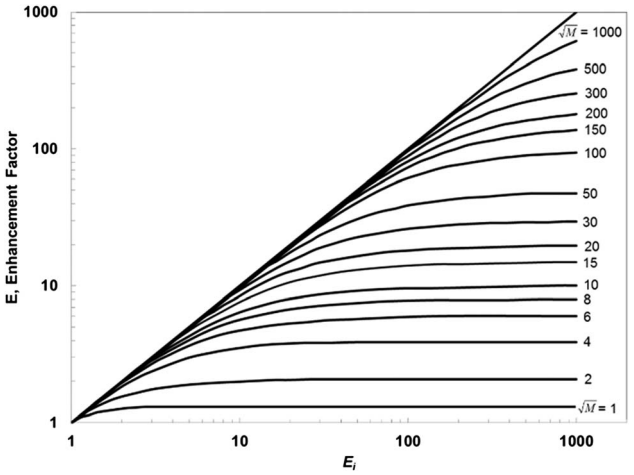

Fig. 1 Enhancement factors for second-order reaction; for use with the film and Higbie models, based on eqn (10).

and the rate of absorption with reaction can be simply approximated by:

$$J_{L,CO_2} = c_i\sqrt{Dkc_B} \quad (14)$$

In terms of the film model, this final definition of the rate of absorption of CO_2 into solution corresponds to a fast pseudo-first-order reaction. In the case in which none of these scenarios hold, the enhancement factor must be obtained from eqn (10) or Fig. 1, after calculation of $\sqrt{M}$ and E_i from eqn (11) and (12), respectively. In the case in which the diffusivity ratio between the binding material and dissolved CO_2, D_B/D, significantly deviates from unity, the Higbie model is recommended over the film model.[21]

3 Potentially tunable solvent parameters for enhancement of mass transfer

Based upon the previous discussion of CO_2 solubility, diffusion in solution, and reaction kinetics, the potentially "tunable" parameters with ranges of values physically achievable today are listed in Table 3. Next, the rate of absorption will be discussed, which relies on knowledge of many of these parameters.

Table 3 Tunable mass-transfer parameters

Parameter	Name	Typical units	Likely range
D_G	Gas diffusivity	$cm^2\ s^{-1}$	0.1–1.0
H	Henry's law constant	atm $cm^3\ mol^{-1}$	11 000–70 000
D	Liquid diffusivity	$cm^2\ s^{-1}$	$(0.5–2.0) \times 10^{-5}$
D_B	Liquid diffusivity of absorbent		
k	Reaction rate constant	L $mol^{-1}\ s^{-1}$	6.7×10^{-4} –1.2×10^{8}
c_B	Bulk concentration of absorbent	mol L^{-1}	0.1–8[a]
k_L	Liquid-phase mass-transfer coefficient	cm s^{-1}	0.001–0.01
c_i	Concentration of CO_2	mol L^{-1}	Set by p_{CO_2} and H
D_B/D	Diffusivity ratio		0.2–2.0

[a] Depending on the corrosive nature, typically less than 1.0 mol L^{-1}.

Table 4 Fluid properties based upon capture application

Application	C_{CO_2} [mol%]	G^a [m s^{-1}]	L^a [m s^{-1}]	$\mu_{gas}{}^{b,c,d}$ [μPa s] × 10^5	$\rho_{gas}{}^{c,d}$ [kg m^{-3}]
Air	0.0004	0.5–2		18.54	1.161
Natural gas plant	3.8	0.5–5	6.63×10^{-4} to 0.005	18.60	1.118
Coal plant	12	0.5–5	0.0023–0.0181	17.97	1.113

[a] Ref. 31 and dependent upon absorber (contactor) diameter. [b] Units of kg m^{-1} s = Pa s. [c] Viscosity and density values are based upon atmospheric pressure and temperatures of 25, 90, and 50 °C for air, natural gas, and coal, respectively. [d] Air, ref. 32 and natural gas/coal, ref. 31.

Published on 25 February 2014. Downloaded by Stanford University on 19/05/2014 02:23:01.

Results and discussion

1 Influence of physical fluid properties on mass transfer

Pressure drop and flooding. The extent of the packing that is ultimately wetted is dependent upon both fluid properties as previously described and process parameters such as gas and liquid flow rates. In fact, both the superficial velocity of the liquid, L, and gas, G, play a role in the process optimization. The superficial velocity of the gas is determined by dividing the volumetric flow rate of the gas for a given application (*i.e.*, natural gas or coal flue gas) by the cross-sectional area of the separation column. The optimal gas velocity is selected to control the pressure drop in the column. There are a number of models that relate the superficial gas velocity to the pressure drop.[60–65] These correlations show that there is a threshold gas velocity, after which the pressure drop sharply increases. Most of the models indicate that at velocities greater than ~2 m s^{-1}, the pressure drop in the column sharply increases above ~2 mbar m^{-1}. This phenomenon occurs because as the gas velocity increases, it forces the liquid to accumulate in the void spaces of the packing material, making it difficult for the gas to flow through. This can ultimately lead to liquid holdup and, eventually flooding of the column. In general, a pressure drop of ~10 mbar m^{-1} corresponds to the flooding point.[31] The superficial gas velocity and subsequent pressure drop can be reduced by increasing the column diameter, which must be done with regard to the liquid flow rate since this will impact the extent to which the packing is wetted. Pressure drop is a primary design component that not only affects the operation of the column, but also influences the required blowing or fan power. The overall pressure drop in a system may include that over gas (air) filtration devices, sorption units, *etc.* Pressure drop is a property that makes the design of a separation unit unique to its application (*i.e.*, DAC *versus* flue gas). For instance, due to the lack of inherent energy in air, a minimal pressure drop is necessary for DAC or else a prohibitive amount of fan energy may be required. To minimize pressure drop the column may be designed to be shorter, and other devices that increase pressure drop, such as air filtration units, should be considered.

Fraction of packing material with wetted surface area. Determining the liquid-phase mass-transfer coefficient first requires investigating the percentage of the packing that is wetted by the solvent, since this dictates the surface area of the interface at which CO_2 transfers from the gas to the liquid phase. The percentage of the packing that is wetted as previously defined is equal to a_w/a_t, such that a_w is the wetted surface area, and a_t is the total packing surface area. From eqn (6), the percentage of wetting depends upon several variables that are a function of the fluid properties, *i.e.*, surface tension (σ), viscosity (μ), and density (ρ).

Based on eqn (6) and the correlation of Onda *et al.*,[28] Fig. 2 shows a plot of the fraction of the surface area wetted as a function of the physical liquid properties surface tension, σ

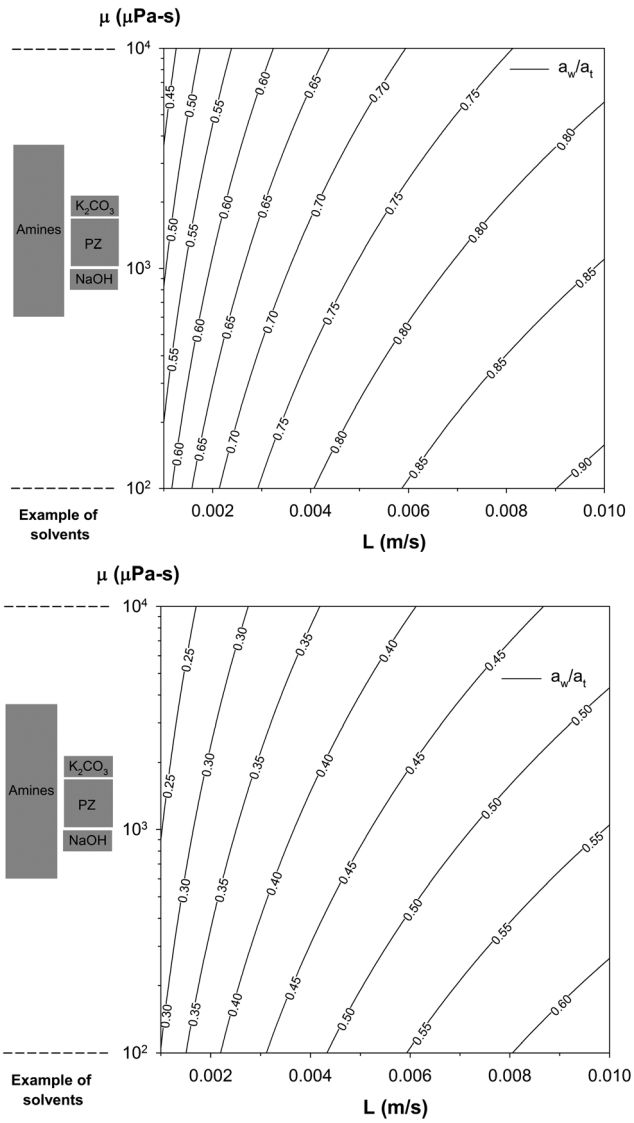

Fig. 2 Fraction of the packing material wetted as a function of solvent viscosity (100 to 10 000 μPa s) and superficial liquid velocity (0.001 to 0.01 m s^{-1}) with a constant fluid density of 1000 kg m^{-3} and surface tension of 0.02 (top) and 0.05 N m^{-1} (bottom).

 This journal is © The Royal Society of Chemistry 2014

Published on 25 February 2014. Downloaded by Stanford University on 19/05/2014 02:23:01.

(0.02 and 0.05 N m^{-1} in Fig. 2, top and bottom, respectively), and viscosity, μ, in addition to the process parameter superficial liquid velocity, L. From Tables 5 and 6 it is clear that the fluid density, ρ, does not vary greatly and was therefore chosen to be constant at 1000 kg m^{-3}. The total packing area, a_t, considered was 500 m^2 m^{-3}, with a critical surface tension, σ_c, of 0.061 N m^{-1}, which is typical for random ceramic packing materials. It is clear from Fig. 2 that the fraction of wetted area increases with decreasing μ and increasing L. The data is presented more explicitly in Table 9. As the fluid viscosity approaches the lower limit of 900 μPa s (*e.g.*, 0.51 M NaOH, 30 °C), the wetted surface area ranges between 19 and 44% over the range of superficial liquid velocities considered (*i.e.*, 0.001–0.01 m s^{-1}). Although the range of possible solvent viscosities is significantly wider than those of the solvent density and surface tension parameters, it turns out that the surface tension, in particular, is a significantly more influential parameter over a small range. For instance, by reducing σ to 0.02 N m^{-1} (Fig. 2, top) from the average of 0.05 N m^{-1} (Fig. 2, bottom), the fraction wetted ranges from ~75% to 90% wetting compared to ~45% to 60% given a superficial liquid velocity of 0.01 m s^{-1} over the same viscosity range of 100–10 000 μPa s. The ultimate goal is to maximize the coverage of the solvent over the packing material in order to increase the interfacial surface area for optimal gas–liquid interaction. Maximizing the percentage of the packing material wetted will provide more opportunities for CO_2 to cross the gas–liquid boundary to ultimately become captured and separated from the gas mixture.

Several solvents from Tables 5 and 6 were explicitly examined with the fraction of wetting, a_w/a_t, presented in Table 9. The general trends for tuning the solvent physical properties to achieve maximum wetting coverage are *decreasing viscosity*, *decreasing surface tension* and *increasing density*. In addition to the currently available solvents displayed in Table 9, a new solvent termed "unobtainium" is listed, with ideal physical properties that would significantly increase the fraction of the packing area wetted. Investigating the list of existing solvents from Tables 5and 6, singling out those with the lowest viscosity (*e.g.*, 10% MDEA, 60 °C), lowest surface tension (*e.g.*, ionic liquid [emim][BF_4]), and highest density (*e.g.*, ionic liquid [emim][Tf_2N]), and enhancing these properties by a factor of two led to the proposed unobtainium solvent. For traditional, existing solvents, the fraction of wetted area ranges from 19% to 51% depending upon the superficial liquid velocity. In the case of the higher liquid velocity of 0.01 m s^{-1}, the fraction of the area wetted using the novel solvent with enhanced physical properties nearly doubles the values of existing solvents. It is also important to note that a_t was chosen as 500 m^2 m^{-3} in the current work, but that the total surface area of various packing materials ranges from the low end in the case of Flexipac-2 (a_t = 233 m^2 m^{-3} with $\varepsilon = 0.95$) to the high end in the case of Mellapack 752Y (a_t = 510 m^2 m^{-3} with $\varepsilon = 0.975$).[66] Investigation of the percentage of the packing area wetted is required to determine the physical liquid-phase mass-transfer coefficient, which is discussed in the next section.

Gas- and liquid-phase mass-transfer coefficients without chemical enhancement. With the exception of the earlier work of Tepe and Dodge[67] and Spector and Dodge,[68] CO_2 absorption studies often neglect mass-transfer resistance in the gas film since it is thought to be negligible compared to the resistance in the liquid film at the gas–liquid interface. Without chemical enhancement of a solvent this assumption is valid over the

Table 5 General solvent liquid-phase physical properties

Solvent [M]	T [°C]	μ [μPa s]	ρ [kg m^{-3}]	σ [N m^{-1}]	Reference
NaOH (30 °C)					
0.91	30	970	1037	0.072	28
0.51		900	1019	0.072	
0.07		810	1001	0.071	
K_2CO_3 (25 °C)					
5.0	25	1900	1241[a]	0.087	33–35
5.0	100	720	978	0.074	
K^+; PZ					
5.0; 2.5	25	4150	1247[a]	—	33
1.0; 1.0		1480	1053[a]	—	
Ionic liquids					
[bmim][PF_6] 4.76 M (100%)	25	1 820 000	1360	0.0488	36 and 37
[bmim][BF_4] 4.89 M (100%)	25	23 300–75 000	1120	0.0466	36–38
[emim][Tf_2N] 3.88M (100%)	25	27 000–28 000	1519	0.0421	36, 37 and 39

[a] Density reported at 0.5, 0.95, 0.667, and 0.25 CO_2 loading, respectively.

Table 6 Amine-based solvent liquid-phase physical properties

Solvent [M]	T [°C]	μ [μPa s]	ρ [kg m^{-3}]	σ [N m^{-1}]	Reference
MEA					
4.1	25	1700	1005.3	0.06263	40
7.0		2200	1010.6	0.06041	41–43
4.1	50	950	994.3	0.05859	40
7.0		1700	1054.5	0.0569	44
DEA					
1.1	20	1427	1010.1	0.06390	45
2.4		2171	1022.0	0.06527	
4.1		3615	1034.2	0.06194	
2.4	60	848	1005.2	0.06204	
4.1		1239	1017.0	0.05802	
MDEA					
0.9	25	1301	1006.2[a]	0.06060	46–48
2.1		1901	1014.4[a]	0.05728	
3.6		3057	1024.9[a]	0.05350	
0.9	60	627	990.4	0.05331	45
2.1		836	997.4	0.05120	
3.6		1119	1004.2	0.04934	
PZ					
1.5	25	1520	1003	0.0717	33 and 49
1.0		1280	1001	0.0701	
0.5		1090	999	0.0693	

[a] Obtained from linear interpolation.

Published on 25 February 2014. Downloaded by Stanford University on 19/05/2014 02:23:01.

majority of conditions. Close examination of the correlations for determining the mass-transfer coefficients in each of the gas and liquid phases leads to the conditions for which this assumption is not valid, even in the absence of chemical enhancement. Recall from eqns (3) and (5) that both the gas- and liquid-phase mass-transfer coefficients depend upon the average diameter of the packing material, d_p, which in turn depends upon the void fraction of the packing, ε. The gas- and liquid-phase mass-transfer coefficients also depend upon fluid properties μ and ρ, as well as the CO_2 diffusivity, D, through the respective fluid, *e.g.*, air, ionic liquid, aqueous amine, *etc.* Similar to the correlation associated with the fraction of the packing material wetted, both mass-transfer coefficient correlations depend upon the superficial gas and liquid velocities, which are parameters of the process, rather than the fluid. Hence, these correlations are quite complex as they include fluid, packing, and process properties.

Fig. 3 shows the relationship between the liquid-phase mass-transfer coefficient, k_L, the superficial liquid velocity, L, and the packing porosity, ε. Since the CO_2 diffusivity through most of the liquid solvents available does not vary significantly, this parameter was assumed fixed at 1×10^{-9} m^2 s^{-1}.[21] Wilke and Chang[69] developed a correlation to estimate gas diffusion in liquids and found a square-root correlation between the gas diffusivity and the molecular weight of the solvent and an inverse correlation between the diffusivity and the solvent viscosity. This indicates that CO_2 diffusion may be significantly hindered in an ionic liquid with a characteristic high viscosity. This effect has not been examined in the current work, but should be explored if these materials are considered for practical applications. It is important to note that the liquid-phase mass-transfer coefficient is also dependent upon both the total surface area, a_t, and the wetted surface area, a_w, as shown in eqn (6). Fig. 3 shows the relationship between the liquid-phase mass-transfer coefficient, packing porosity, ε, and superficial

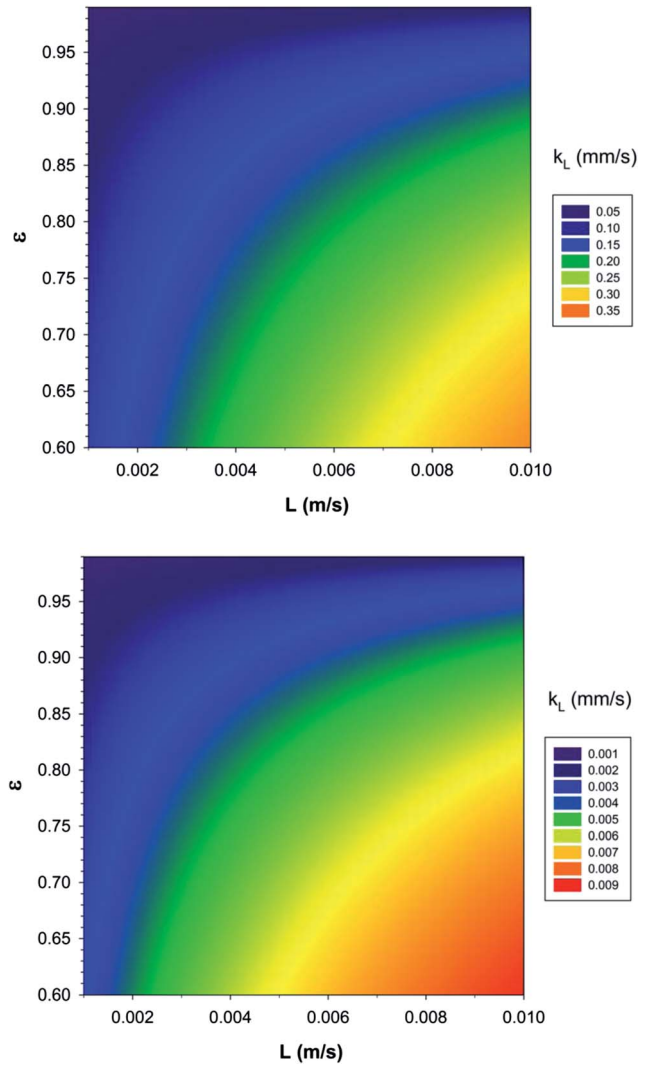

Fig. 3 Liquid-phase mass-transfer coefficient displayed as a function of packing porosity, ε (0.6–0.99), and superficial liquid velocity, L (0.001–0.01 m s^{-1}), with surface tension constant at 0.05 N m^{-1} and minimum viscosity of 100 μPa s (top) and 10 000 μPa s (bottom). The bottom plot shows k_L values associated with ionic liquids.

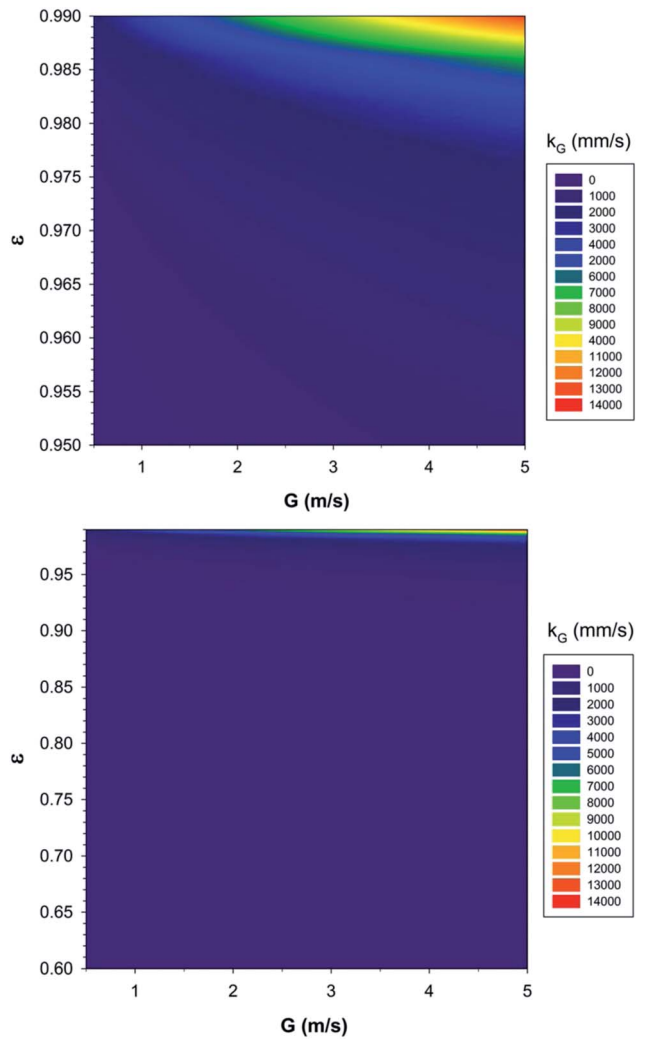

Fig. 4 Gas-phase mass-transfer coefficient displayed as a function of packing porosity, ε (top, 0.95–0.99; bottom, 0.60–0.99), and superficial gas velocity, G (0.5–5), with surface tension constant at 0.05 N m^{-1}, viscosity of 18 μPa s, density of 1.1 kg m^{-3} and CO_2 diffusivity of 1.65×10^{-5} m^2 s^{-1}.

This journal is © The Royal Society of Chemistry 2014

Published on 25 February 2014. Downloaded by Stanford University on 19/05/2014 02:23:01.

liquid velocity, L, for a fluid with a density of 1000 kg m^{-3} and a surface tension of 0.05 N m^{-1}. Depending upon the liquid-phase superficial velocity (0.001–0.01 m s^{-1}) and the packing void fraction (0.6–0.99), k_L varies from 0.05 to 0.25 mm s^{-1} for a fluid having a viscosity of 100 μPa s (Fig. 3, top) and from 0.001 to 0.006 mm s^{-1} for a fluid with a viscosity of 10 000 μPa s (Fig. 3, bottom).

Fig. 4 shows the relationship between the gas-phase mass-transfer coefficient and the superficial gas velocity, G, and packing porosity, ε. Gases from which CO_2 separation may take place include flue gases generated from natural gas- and coal-fired utilities and air. Recalling the density and viscosity properties of these gases listed in Table 4, it is clear that they are quite similar. Therefore, a gas viscosity of 18 μPa s and density of 1.1 kg m^{-3} was assumed for the gas-phase mass-transfer coefficients plotted in Fig. 4. Also, it was assumed that the CO_2 diffusivity would likely be fairly similar for each of these gases and so was fixed at 1.65×10^{-5} m^2 s^{-1}.[12] This data is also listed explicitly in Table 10. Depending upon the superficial gas velocity and the packing porosity, k_g may vary between ~10 mm s^{-1} and ~130 mm s^{-1}.

An important observation can be made between the rate of CO_2 transfer in the gas *versus* liquid phases through a packed bed based upon a comparison of various liquids and gases, as presented in terms of the liquid and gas-phase mass-transfer coefficients, expressed in units of mm s^{-1} in Table 10. In general, the liquid-phase mass-transfer of CO_2 is faster in material with a smaller void fraction, while the gas-phase mass-transfer is faster in material with a higher void fraction. There are no scenarios from Table 10 in which the gas-phase mass-transfer coefficient is not at least two orders of magnitude greater than the liquid-phase mass-transfer coefficient. Therefore, it can be generally concluded that the gas-phase resistance may be neglected for conditions in which chemical enhancement is not included. However, since CO_2 capture from flue gas and air will likely take place with chemical enhancement, it is more useful to compare the chemically-enhanced k_L to k_G to determine the regimes under which mass transfer is limited and to consider the relative resistance in the gas *versus* the liquid film. It is should be noted that the values reported in Table 10 for k_L and k_G are consistent with those reported in previous correlation studies.[31]

2 Influence of chemical fluid properties on mass transfer

Determining how chemical enhancement plays a role in increasing the flux of CO_2 across the gas–liquid interface requires calculation of the instantaneous enhancement factor, E_i, and the parameter $\sqrt{M}$. E_i is a thermodynamic parameter that primarily depends upon the initial CO_2 gas concentration, while $\sqrt{M}$ depends primarily on the reaction kinetics associated with CO_2 and the solvent binding chemical, with complete disregard to the initial CO_2 concentration. These two parameters determine how the flux equation is defined, which describes CO_2 transport across the interface. Each of these parameters will be described in detail for various CO_2 gas mixtures and the resulting flux equations will be discussed.

Instantaneous enhancement factor (E_i) – relies upon the initial CO_2 gas concentration. Investigation of the enhancement effect of a chemical reaction between CO_2 and a binding species

Table 7 General solvent liquid-phase chemical properties

Solvent [M]	T [°C]	H [atm cm^3 mol^{-1}]	H^a	k [cm^3 mol^{-1} s^{-1}] × 10^{-6}	Reaction mechanisms for CO_2 capture	Reference
NaOH						
0.91	30	44 248	0.562	9.92	$CO_2 + OH^- \rightarrow HCO_3^-$	28
0.51		39 370	0.631	8.75	$HCO_3^- + OH^- \rightarrow CO_3^{2-} + H_2O$	
0.07		34 364	0.723	7.67		
K_2CO_3						
2.71	25	152 440	0.160	10[b]	$CO_2 + CO_3^{2-} + H_2O \leftrightarrow 2HCO_3^-$	33, 35 and 50
1.17		65 890	0.371	—		
5.0	100	153 397	0.199	3200[b]		
K_2CO_3; PZ						
0.54; 1.09	25	42 970	0.569	—	$CO_2 + CO_3^{2-} + H_2O \leftrightarrow 2HCO_3^-$	33 and 51
1.07; 1.07		62 030	0.394	—		
3.6 K^+; 0.6 PZ		65 890	0.371	47.0		
$Ca(OH)_2$						
0.023	25	30 840[c]	0.792	10	$CO_2 + 2HO^- \leftrightarrow CO_3^{2-} + H_2O$	52
Ionic liquids						
[bmim][PF_6] 4.76 M (100%)	30	14 286	1.740	N/A	Physical solubility	53
[emim][TfO] 5.32M (100%)	30	12 500	1.989			
[emim][Tf_2N] 3.88M (100%)	30	11 111	2.237			

[a] Calculated from dimensional H by: H[dimensionless] = R[cm^3 atm K^{-1} mol^{-1}] × T[K]/H[atm cm^3 mol^{-1}], where R is the gas constant and .R = 82 cm^3 atm K^{-1} mol^{-1}. [b] Reported for the rate-limiting reaction: $CO_2 + OH^- \leftrightarrow HCO_3^-$ with [K^+] = 4.5 M. [c] Henry's law constant for the CO_2(g)/H_2O(l) system at 25 °C, adapted from ref. 52.

Published on 25 February 2014. Downloaded by Stanford University on 19/05/2014 02:23:01.

Table 8 Solvent liquid-phase chemical properties at 25 °C

Solvent [M]	H [atm cm^3 mol^{-1}]	H^a	k [cm^3 mol^{-1} s^{-1}] × 10^{-6}	Reaction mechanisms for CO_2 capture	Reference
MEA					
2.0	31 404	0.778	5.87	$CO_2 + RNH_2 \leftrightarrow RNH_2^+CO_2^-$	42 and 54–56
2.5	31 503	0.776		$RNH_2^+CO_2^- + H_2O \rightarrow RNHCO_2^- + H_3O^+$	
3.0	31 700	0.771		or $CO_2 + RNH_2 + H_2O \leftrightarrow RNHCO_2^- + H_3O^+$, where R = C_2H_4OH	
DEA					
2.0	37 375	0.654	1.25	$CO_2 + R_2NH \leftrightarrow R_2NH^+CO_2^-$	43, 54–56
2.5	38 095	0.641		$R_2NH^+CO_2^- + H_2O \rightarrow R_2NCO_2^- + H_3O^+$ or	
3.0	39 171	0.624		$CO_2 + R_2NH + H_2O \leftrightarrow R_2NCO_2^- + H_3O^+$, where R = C_2H_4OH	
MDEA					
2.0	34 483	0.709	0.0055	$R_2R'N + H_2O \leftrightarrow R_2R'NH^+ + OH^-$	43, 57 and 58
2.5	36 526	0.669		$OH^- + CO_2 \leftrightarrow HCO_3^-$ where R = C_2H_4OH,	
3.0	37 908	0.645		R′ = CH_3	
PZ					
0.57	30 360	0.805	53.7	$CO_2(aq) + 2H_2O \leftrightarrow HCO_3^- + H_3O^+$	33 and 59
1.09	29 910	0.817		$HCO_3^- + H_2O \leftrightarrow CO_3^{2-} + H_3O^+$	
1.56	31 600	0.773		$PZ + H_2O + CO_2(aq) \leftrightarrow PZCO_2^- + H_3O^+$	
				$PZH^+ + H_2O \leftrightarrow PZ + H_3O^+$	
				$PZCO_2^- + H_2O + CO_2(aq) \leftrightarrow PZ(CO_2^-)_2 + H_3O^+$	
				$H^+PZCO_2^- + H_2O \leftrightarrow PZCO_2^- + H_3O^+$	

[a] Calculated from dimensional H by: H[dimensionless] = R[cm^3 atm K^{-1} mol^{-1}] × T[K]/H[atm cm^3 mol^{-1}], where R is the gas constant and R = 82 cm^3 atm K^{-1} mol^{-1}.

present in the solvent requires knowledge about the binding species itself and the mechanism of the reaction. The two possible reaction mechanisms as outlined in detail in Tables 7 and 8 are carbonate and carbamate chemistries. The enhancement factor can be determined by eqn (10). However, as outlined in Table 2, there are simplified expressions for the enhancement factor, depending upon the reaction conditions. To examine the validity of these conditions for a given scenario, the terms E_i and $\sqrt{M}$ must first be calculated. From eqn (12), determining E_i depends upon the ratio of the base to CO_2 diffusivity in solution, the stoichiometric ratio of the chemical reaction and, most importantly, on the interfacial concentration, c_i.

Eqn (12) can be rewritten in the following simplified form:

$$E_i = \left(1 + \frac{D_B c_B}{z D c_i}\right) = \left(1 + \frac{D_s c_B}{c_i}\right) \quad (15)$$

such that $D_s = D_B/zD$, and is typically considered equal to 1/2, 1, or 2. It was determined that c_i is the most sensitive and tunable parameter from the calculation of E_i, given the physical ceiling typically placed on c_B due to the increasing corrosive nature associated with the increase in base concentration in solution.

Since the interfacial concentration is dependent upon Henry's law and hence the partial pressure of CO_2 in equilibrium with the solvent, it is important to consider the various applications (*i.e.*, DAC *versus* flue gas from coal or natural gas) separately. Recall from Tables 7 and 8, for either carbonate or carbamate formation pathways, the Henry's law constant for the various solvents ranges from the most soluble at ~30 000 atm cm^3 mol^{-1} for a 0.023 M $Ca(OH)_2$ solution to the least soluble at ~150 000 atm cm^3 mol^{-1} for a 2.71 M K_2CO_3 solution. It is important to note that ionic liquids have enhanced solubility over the other chemical solvents reported; however, the mechanism of CO_2 transfer into the ionic liquid is driven by physical solubility with no chemical enhancement. Ionic liquids are discussed as a special case and in greater detail later. Fig. 5 shows a plot of two partial pressure ranges with DAC labeled in the top plot and natural gas- and coal-fired flue gas labeled accordingly in the bottom plot. As expected, the maximum

Table 9 Fraction of packing material wetted for several existing solvents and an optimal "unobtainium" solvent

Solvent	μ [μPa s]	ρ [kg m^{-3}]	σ [N m^{-1}]	a_w/a_t L = 0.001 m s^{-1}	a_w/a_t L = 0.01 m s^{-1}
NaOH, 30 °C, 0.51 M	900	1019	0.071	0.19	0.44
MEA, 25 °C, 30%	2200	1011	0.0604	0.20	0.46
[emim][BF_4], 25 °C, 4.89 M	23 300	1120	0.0466	0.22	0.51
Unobtainium (2×)[a]	400	2000	0.02	0.60	0.95

[a] 2× notation refers to the optimal solvent "unobtainium" with properties of decreased viscosity and surface tension, and increased density from the top-performing existing solvents, by a factor of two.

 This journal is © The Royal Society of Chemistry 2014

Published on 25 February 2014. Downloaded by Stanford University on 19/05/2014 02:23:01.

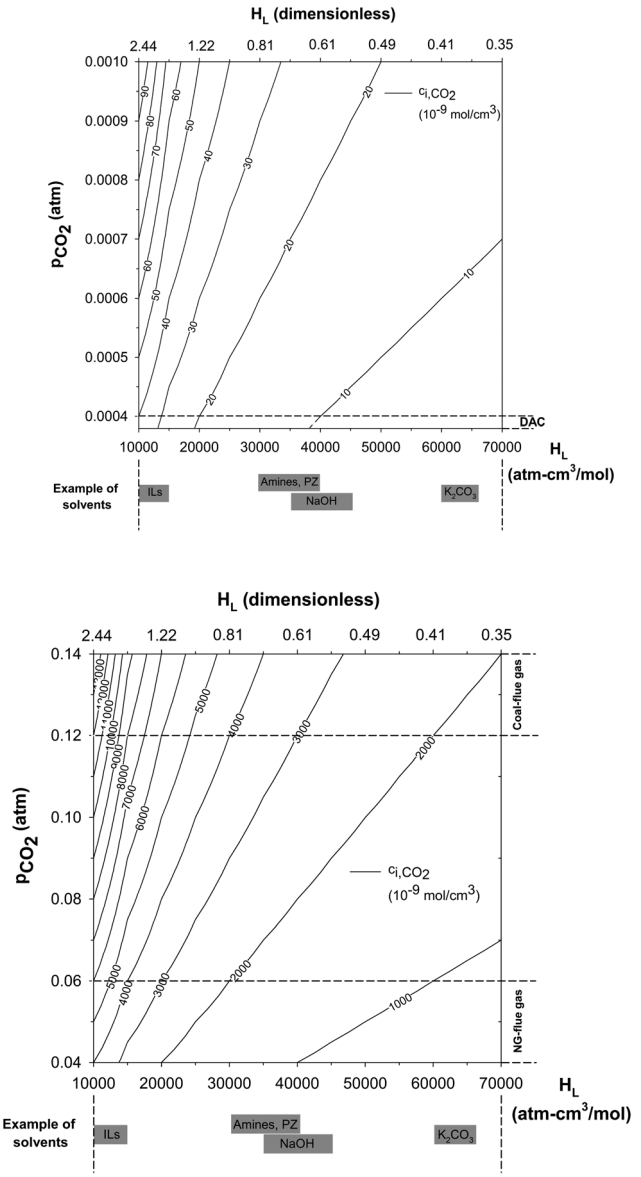

Fig. 5 Interfacial concentration of CO_2 as a function of CO_2 partial pressure between 0.0004–0.001 atm (top) and 0.04–0.14 atm (bottom) and Henry's law constant between 10 000–70 000 atm cm^3 mol^{-1}, spanning that of ionic liquids to potassium carbonate.

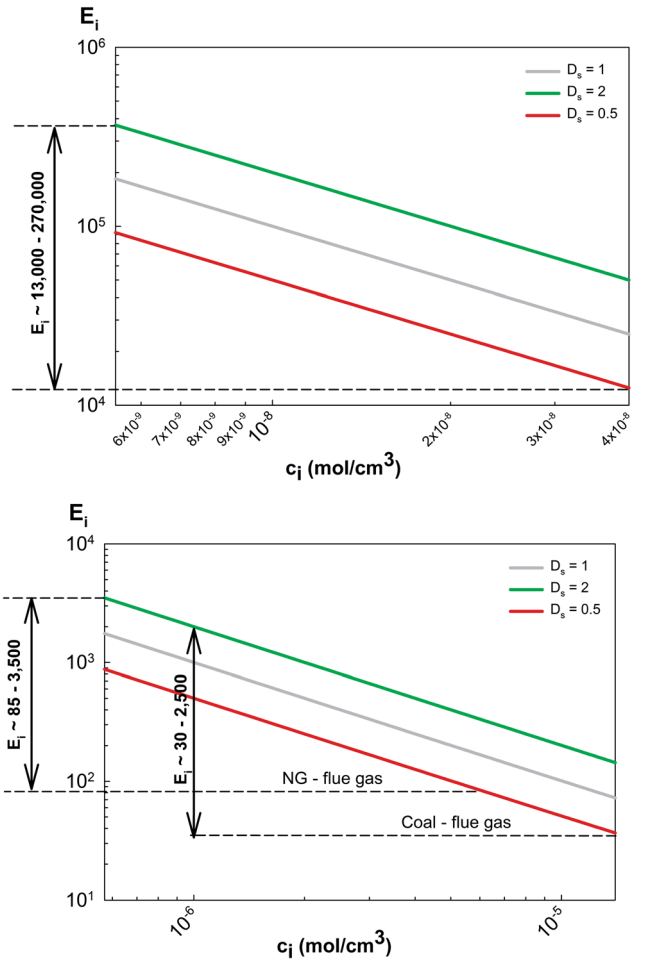

Fig. 6 Instantaneous enhancement factor as a function of interfacial CO_2 concentration for applications ranging from DAC (top) to flue gas from natural gas- or coal-fired power plant (bottom).

achievable interfacial concentration of CO_2 is obtained at the highest CO_2 partial pressure (*i.e.*, flue gas from coal combustion) and using a highly CO_2-soluble solvent with H ~10 000 atm cm^3 mol^{-1}. As shown along the *x*-axis in Fig. 5, ionic liquids are the only solvents that exhibit such high CO_2 solubilities.

It is also important to note that due to the limitation of dilute solutions (*i.e.*, DAC), the interfacial CO_2 concentration exhibits a maximum of ~3×10^{-8} mol cm^{-3} *versus* the more concentrated system (*i.e.*, coal flue gas) of ~1.4×10^{-5} mol cm^{-3}. That the flux of CO_2 across the gas–liquid interface is directly proportional to the product of the interfacial CO_2 concentration and the liquid-phase mass-transfer coefficient, which is purely a property of the process and liquid-phase physical properties, highlights the importance of the Henry's law constant in solvent design. However, in a chemically-enhanced process the product $c_i k_L$ is multiplied by an enhancement factor, E, which is determined based upon satisfaction of a set of conditions as described in Table 2.

Fig. 6 shows the relationship of E_i and c_i with an assumed base concentration (c_B) of 0.001 mol cm^{-3} and a series of D_s values as previously described. Also, from Fig. 6 it is interesting to note the large difference between E_i for DAC (*i.e.*, 13 000–270 000) and natural gas- (*i.e.*, 85–3500) or coal-fired (*i.e.*, 30–2500) flue gas cases. In fact, E_i is always much larger than $\sqrt{M}$ in the case of DAC, indicating that DAC will proceed *via* a pseudo-first-order or fast pseudo-first-order reaction. Alternatively, in the case of coal-fired flue gas, there are some conditions where CO_2 uptake occurs instantaneously.

Parameter $\sqrt{M}$ – relies upon solvent and process properties. At this stage it is important to recall the relationship between $\sqrt{M}$ and E_i as shown in Table 2. All cases considered in this discussion either fall into the Limiting Case #1, in which $\sqrt{M} > 10E_i$, or the Limiting Case #3, in which $\sqrt{M} < 1/2E_i$ and $\sqrt{M} > 3$. The flux equation that describes the transport of CO_2 across the gas–liquid boundary is different in each of these cases. In the Limiting Case #1, the CO_2 flux is $c_i k_L E_i$, while in the Limiting Case

Published on 25 February 2014. Downloaded by Stanford University on 19/05/2014 02:23:01.

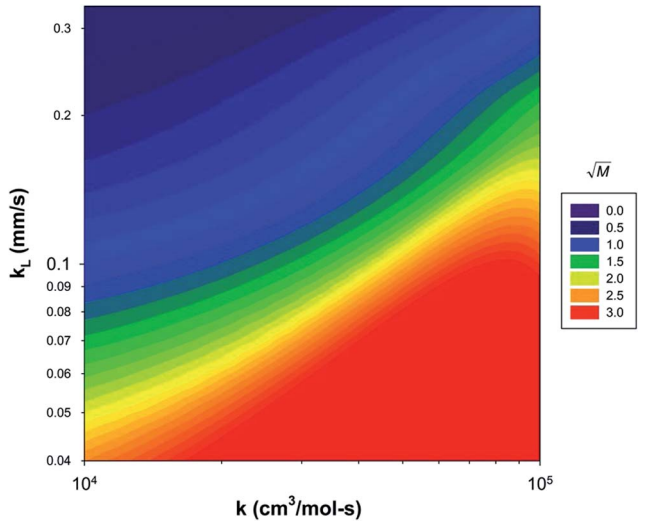

Fig. 7 Calculation of $\sqrt{M} < 3$ as a function of the liquid-phase mass transfer coefficient, k_L and rate constant, k.

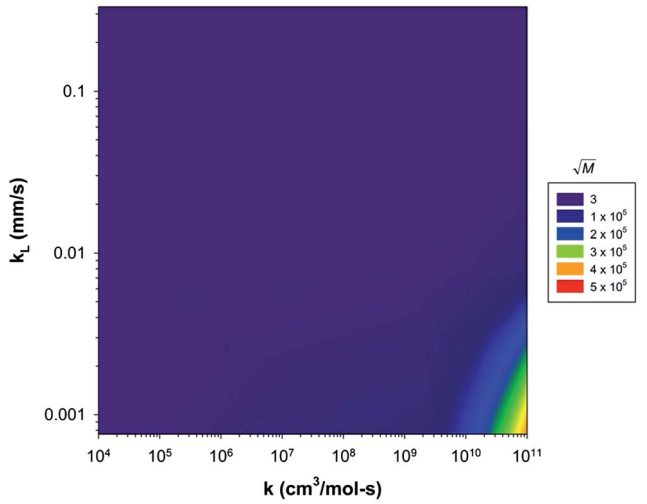

Fig. 8 Dependence of $\sqrt{M}$ on liquid-phase mass-transfer coefficient, k_L, and rate constant, k, ranging from 10^4 to 10^{11} cm^3 mol^{-1} s^{-1}.

#3, the CO_2 flux is $c_i\sqrt{Dkc_B}$. Fig. 7 shows the conditions of the liquid-phase mass-transfer coefficient, k_L, and rate constant, k, that give rise to $\sqrt{M} < 3$. A solvent that would lead to this condition would have a viscosity significantly lower than the average (*i.e.*, 100 μPa s) and a low rate constant. From Tables 7 and 8, the solvent MDEA is the only one that fits these criteria.

Fig. 8 shows the dependence of $\sqrt{M}$ on k_L and k, with the rate constant described over the range of 10^4 to 10^{11} cm^3 mol^{-1} s^{-1}, which includes all of the solvents in Tables 7 and 8, assuming a range of reasonable viscosities that lead to k_L ranging between 0.001 and ~0.1 mm s^{-1}. In particular, the upper range, *i.e.*, 10^7 to 10^{11} cm^3 mol^{-1} s^{-1}, assumes a transformational improvement in the rate constant due to the presence of carbonic anhydrase.[12] This plot reveals that the majority of the conditions lead to $\sqrt{M}$ values greater than 3, which becomes important considering the cases outlined in Table 2.

Instantaneous reaction conditions. In the case of an instantaneous reaction in which $E = E_i$, only the thermodynamics play a role in determining the CO_2 flux. For example, a $\sqrt{M}$ 10 times larger than E_i indicates a large $\sqrt{M}$ (*i.e.*, small k_L and/or high k) and/or a small E_i (*i.e.*, c_i is large). The cases of small k_L and large c_i both result in an accumulation of CO_2 in the liquid film or boundary of the liquid phase, indicating that when a CO_2 molecule reacts and leaves the region of the interface, there is another CO_2 molecule in place to react. Hence, the capture (CO_2 binding reaction) is described as being instantaneous. Let us consider the conditions that would lead to an instantaneous reaction. In the case of DAC, where E_i may range between 13 000 and 270 000, due to the low partial pressure CO_2 in the atmosphere, $\sqrt{M}$ must be greater than 1.3×10^5 to 2.7×10^6, respectively. For the lower range of E_i, a solvent with a rate constant greater than or equal to 1×10^{10} cm^3 mol^{-1} s^{-1} and with k_L less than or equal to 1×10^{-3} mm s^{-1} would result in an instantaneous reaction. Importantly, this would render the dilute DAC system comparable to a concentrated CO_2 gas mixture in terms of CO_2 flux, recalling that the CO_2 flux for the instantaneous case is $c_i k_L E_i$. In this case the low c_i of DAC is offset by the extremely high E_i (*i.e.*, 13 000–270 000), which is inversely proportional to c_i by eqn (12). In the case of natural gas flue gas, an instantaneous reaction would occur with $\sqrt{M} > 850$ to 35 000. At the low 850 range (see Fig. 6, bottom) this occurs with $k > 1 \times 10^6$ cm^3 mol^{-1} s^{-1} and $k_L < 1 \times 10^3$ mm s^{-1}, with k_L allowed to increase as k increases. In the case of coal flue gas, the conditions require $\sqrt{M} > 300$ to 25 000 to meet the instantaneous reaction criterion. This occurs with k as low as low as 1×10^5 cm^3 mol^{-1} s^{-1} and $k_L < 1 \times 10^3$ mm s^{-1}.

Fast pseudo-first-order reaction conditions. In the case of a fast pseudo-first-order reaction, $E = \sqrt{Dkc_B}$, and the subsequent CO_2 flux across the interface is $c_i\sqrt{Dkc_B}$. The requirements for this Limiting Case #3 are that $\sqrt{M} < 1/2E_i$ and that $\sqrt{M} > 3$, from Table 2. As previously outlined, the only solvent examined in this work that leads to $\sqrt{M} < 3$ is MDEA, indicating that most solvents will satisfy the criterion of $\sqrt{M} > 3$, in that the chemical binding reaction takes place at a moderate rate. Hence, MDEA is one of the few solvents that proceeds *via* a pseudo-first-order

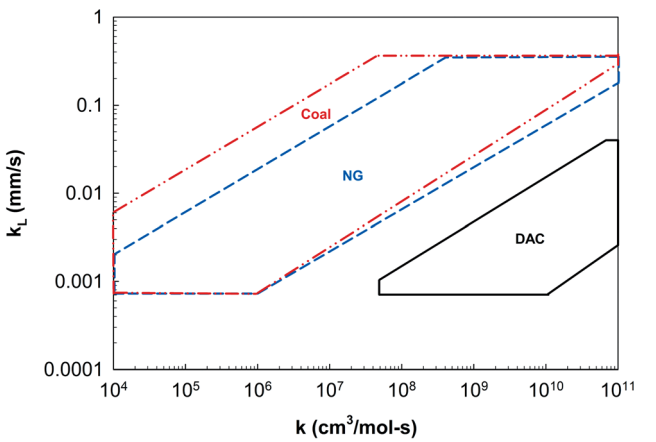

Fig. 9 Conditions (k and k_L) for which Limiting Case #3 (Table 2) does not apply and full film model must be used.

This journal is © The Royal Society of Chemistry 2014

Published on 25 February 2014. Downloaded by Stanford University on 19/05/2014 02:23:01.

reaction, and is not considered *fast*, in other words that satisfies the Limiting Case #2 from Table 2. Fig. 9 shows all the scenarios in which the Limiting Case #3 is *not* satisfied for DAC and flue gases from natural gas- and coal-fired power utilities. These scenarios are cases in which $\sqrt{M} > 1/2E_i$ and as such the full film model must be applied and eqn (9) used to accurately calculate the enhancement factor, E.

Implications of always assuming fast pseudo-first-order reaction. From Fig. 9 it is clear that as solvents become more advanced in terms of their kinetic enhancement, the assumption of fast pseudo-first-order is likely to be an inaccurate assumption. To investigate the impact that this assumption has on the calculation of the CO_2 flux, conditions were chosen that lie in the regions of Fig. 9 for the case of coal-fired flue gas and using a 0.51 M solution of NaOH at 25 °C. Table 11 shows a comparison of the flux calculated using the Higbie model (*i.e.*, *Higbie J*) using eqn (16) for the calculation of E_i; E as defined in the Limiting Case #3 (*i.e.*, *Film 3J*) and given in eqn (13); and the full film model (*i.e.*, *Full Film J*) as given in eqn (10).

$$E_i \approx \sqrt{\frac{D}{D_B}} + \frac{c_B}{z c_i}\sqrt{\frac{D_B}{D}} \quad (16)$$

Properties of the solvent were taken from Tables 5 and 7, with the process parameter $L = 0.001$ m s^{-1} and a viscosity of 100 μPa s. Values of k_L listed for each set of conditions were calculated using eqn (5) and (6).[25] In general, the flux estimates are quite similar regardless of assuming the Limiting Case #3 and eqn (13) for the calculation of the enhancement factor. However, it is anticipated that as solvents are designed with k and k_L conditions that lie deep within the regions shown in Fig. 9, the error associated with assuming the fast pseudo-first-order reaction will be greater; therefore, the use of the full film model is strongly encouraged for the conditions shown in Fig. 9.

Liquid-phase mass-transfer coefficient (k_L) discrepancies in the literature. Recent studies have used the liquid-phase mass-transfer coefficient to estimate the required design parameters for absorption columns for applications of DAC and flue gas from natural gas and coal combustion. In order to avoid confusion between the k_L estimated in the current work and those previously reported, attention is given to the various assumptions made that lead to discrepancies in these values. A recent review carried out by Razi, Bolland, and Svendsen[31] focused on the design correlations specifically for CO_2 absorption into MEA using structured packings. This work explored the various correlations developed for wetting, gas- and liquid-phase mass-transfer, and pressure drop correlations as applied to flue gas from natural gas- and coal-fired power plants. Of the 10+ correlations considered for liquid-phase mass-transfer coefficient estimates, only one fell outside of the range of 0.01–0.1 mm s^{-1} for both flue gas applications. These estimates are consistent with the current work, but inconsistent with others reported in the literature. A recent study published by Holmes and Keith[23] on the design parameters of an air–liquid contactor for large-scale capture of CO_2 from air provided a review of previously published liquid-phase mass-transfer coefficients, with values 1–2 orders of magnitude greater than those of the current work and that of Razi *et al.*[31] The reason for these higher values is due to the difference in how the authors defined the mass-transfer coefficient. It appears that in their definition they included the dimensionless Henry's law constant, which leads to increased values due to different units. Dividing the mass-transfer coefficient values reported in their work by the

Table 10 Comparison of liquid- and gas-phase mass-transfer coefficients for a variety of conditions *without* chemical enhancement

Fluid	μ[μPa s]	ρ[kg m^{-3}]	σ[N m^{-1}]	k [mm s^{-1}] $\varepsilon = 0.75$; 0.90	
Liquids				$\boldsymbol{L = 0.001}$ **m s^{-1}**	$\boldsymbol{L = 0.01}$ **m s^{-1}**
NaOH, 30 °C, 0.51 M	900	1019	0.071	0.119; 0.082	0.320; 0.219
MEA, 25 °C, 7.0 M	2200	1010.6	0.0604	0.108; 0.075	0.297; 0.204
[emim][BF_4], 25 °C, 4.89 M	23 300	1120	0.0466	0.003; 0.002	0.008; 0.005
Unobtainium	400	2000	0.02	0.104; 0.071	0.374; 0.257
Gases				$\boldsymbol{G = 2.0}$ **m s^{-1}**	$\boldsymbol{G = 5.0}$ **m s^{-1}**
Air	18.54	1.161	NA	10.1; 62.9	20.9; 131
Coal-fired flue gas	18.6	1.118	NA		
Natural gas-fired flue gas	17.97	1.113	NA		

Table 11 Comparison of CO_2 fluxes using various models for a 0.51 M NaOH solution at 25 °C

ε	D_B/D	k_L [mm s^{-1}]	Higbie J [mol cm^{-2} s^{-1}] × 10^6	Film 3 J [mol cm^{-2} s^{-1}] × 10^6	Full Film J [mol cm^{-2} s^{-1}] × 10^6	J error[a] [%]	J error[b] [ratio]
0.9	1	0.068	1.46	1.56	1.25	25	1.25
0.9	2	0.068	2.05	1.56	1.40	12	1.1
0.6	1	0.118	2.53	1.56	1.38	13	1.1

[a] Defined as (Film 3J − Full Film J)/Full Film J. [b] Defined as Film 3J/Full Film.

Table 12 Comparison of gas- and liquid-phase mass-transfer resistances

k_g [mm s^{-1}]	k_L [mm s^{-1}]	"Ek_L" $= \sqrt{Dkc_B}$[e] [mm s^{-1}]	H	H/k_L[h] [s mm^{-1}]	H/Ek_L[h] [s mm^{-1}]	$1/k_g$ [s mm^{-1}]
1000[a]	0.001[c]	1.0 ($k = 1 \times 10^6$ cm^3 mol^{-1} s^{-1})	0.1[f]	0.285	3.16×10^{-4}	0.001
13 000[b]	0.35[d]	316 ($k = 1 \times 10^{11}$ cm^3 mol^{-1} s^{-1})	2.2[g]			7.6×10^{-6}

[a] $\varepsilon < 0.98$ and $G = 1$–5 m s^{-1}. [b] $\varepsilon > 0.98$ and $G > 2.5$ m s^{-1}. [c] $\varepsilon > 0.6$ and $L < 2$ mm s^{-1}; $\varepsilon > 0.85$ and $L > 4$ mm s^{-1}. [d] $0.6 < \varepsilon < 0.65$ and $L > 9$ mm s^{-1}. [e] $D = 1 \times 10^{-5}$ cm^2 s^{-1} and $c_B = 1 \times 10^{-3}$ mol cm^{-3}. [f] Potassium carbonate. [g] Ionic liquids. [h] Divided extremes to determine greatest extent of resistance.

Published on 25 February 2014. Downloaded by Stanford University on 19/05/2014 02:23:01.

dimensionless H as given in Tables 7 and 8 yields estimates in line with those of the current work.

Another common problem is the confusion between the *physical* and the *chemically-enhanced* liquid-phase mass-transfer coefficient. When parameters such as base concentration and rate constant are used in the calculation, this implies the inclusion of chemical enhancement and, as expected, results in a larger value of k_L. Table 12 shows *physical* k_L *versus enhanced* k_L for two different scenarios, *i.e.*, moderate (1×10^6 cm^3 mol^{-1} s^{-1}) and very fast (1×10^{11} cm^3 mol^{-1} s^{-1}) chemical reactions. The enhanced liquid-phase mass-transfer coefficients range from 1.0 to 316 mm s^{-1}, indicating the possible range of the parameter space of this coefficient and its dependence upon the rate of the chemical reaction. Likely some of the studies cited in Holmes and Keith[23] are representative of enhanced mass transfer with a chemical reaction, rather than simply physical mass transfer, which would be based primarily on solubility and Henry's law.

The recent work of Mazzotti *et al.*[24] focused on the optimization of a process for DAC of CO_2 and reported enhanced k_L. In addition, they chose an alternate definition (reverse) of Henry's law from that of the current work and that of Holmes and Keith.[23] In the study carried out by Mazzotti *et al.*,[24] the Henry's law constant was defined as the ratio between the interfacial concentration of CO_2 and its partial pressure in the gas phase, resulting in H multiplied by RT and k_L in the denominator of the liquid-phase resistance term of the overall mass-transfer resistance equation (eqn (1) of current work).

When does gas-phase resistance begin to play a role? Recall eqn (1) in which the overall mass-transfer resistance is comprised of the resistance associated with mass transfer in the gas phase and the resistance in the liquid phase. It is commonly assumed that mass-transfer resistance is dominant in the liquid film and it was shown previously in Fig. 3 and 4 through a direct comparison between k_g and k_L that this is the case in the absence of chemical enhancement. Table 12 verifies this by listing extremes of k_g and physical k_L along with their reciprocals (resistance form) in accordance with eqn (1). In examining the enhancement of the liquid-phase mass-transfer coefficient, only the Limiting Case #3 from Table 2 was considered as it represents the broadest range of conditions. Considering a solvent with low CO_2 solubility (2.71 M K_2CO_3 at 25 °C) and kinetics on the order of carbonic anhydrase results in conditions in which the resistance of CO_2 transfer in the liquid is minimized and hence is comparable to gas-phase resistance estimates. Although these conditions may seem rare, it is important to keep in mind that with the advent of new solvents with improved kinetics, both gas- and liquid-phase resistances have the potential to play a role in determining the overall mass-transfer coefficient.

Special solvent case – ionic liquids and why they work. Ionic liquids are an interesting case in that they are fairly competitive with traditional aqueous-based solvents, but they operate *via* a physical rather than a chemical mechanism. From Table 7 and Fig. 5 it is clear that ionic liquids exhibit the highest CO_2 solubility among all of the solvents considered. Revisiting the general flux equation without chemical enhancement, $J = c_i k_L$, one can readily see that the flux is directly proportional to the interfacial concentration, which is significantly higher in the case of ionic liquids compared to the traditional aqueous-based solvents. However, due to limitations in their physical properties (*i.e.*, σ, ρ, and μ), they are not able to wet packing material as efficiently as aqueous-based solvents and hence have a significantly lower k_L, primarily due to their high viscosity as shown in Fig. 3 (bottom). Ultimately there is a balance between their high solubility for CO_2 and low liquid-phase mass-transfer coefficient that results in their product, *i.e.*, CO_2 flux, being competitive with traditional solvents that typically exhibit moderate solubilities and fairly tunable k_L.

Summary and future directions on tuning solvents for varying levels of dilution

Film theory and mass-transfer correlations were revisited to determine the solvent and process parameters most influential for CO_2 capture. Specifically, the two primary flux equations, *i.e.*, $J_{CO_2} = k_L c_i E$ and $J_{CO_2} = c_i \sqrt{Dkc_B}$, were examined in detail to identify the most important parameters for maximizing CO_2 flux across the gas–liquid interface. The second flux equation is used for fast pseudo-first-order reactions by the criteria outlined in the Limiting Case #3 of Table 2, while the first equation applies to all other scenarios. The results of the current work indicate that the primary tunable parameters for enhancing CO_2 flux in carbon capture applications are c_i, k_L, and k. Both c_i and k are solvent parameters; however, c_i is a thermodynamic parameter independent of the time scale, while k is a kinetic parameter independent of equilibrium. On the other hand, k_L has both process and solvent property origins as it is dependent upon the process parameters L and ε, and the physical parameters of a solvent σ, ρ, and μ. Each of these tunable parameters will be discussed in turn along with the three carbon capture applications of focus, *i.e.*, DAC and flue gases from natural gas- and coal-fired power plants.

 This journal is © The Royal Society of Chemistry 2014

Published on 25 February 2014. Downloaded by Stanford University on 19/05/2014 02:23:01.

(1) Increasing the interfacial CO_2 concentration, c_i leads to enhanced CO_2 capture. According to Fig. 5, over the full range of solvents considered (aqueous-based to ionic liquids), the ranges of c_i are 0.01×10^{-6} to 0.04×10^{-6} mol cm^{-3} for DAC, 1.0×10^{-6} to 6.0×10^{-6} mol cm^{-3} for natural gas and 2.0×10^{-6} to 12×10^{-6} mol cm^{-3} for coal applications. For similar solvents, the interfacial concentration of CO_2 for DAC is 100 times less than natural gas, which is half that of coal flue gas. However, using ionic liquids for DAC and an aqueous-based solvent for natural gas results in a c_i for the natural gas case only 25 times more concentrated than the DAC case. As previously discussed and demonstrated in Fig. 2, the wetting properties of ionic liquids are limited. Hence, an improvement in solvent design may be a hybrid fluid approach in which the highly soluble phase prefers to exist along the gas–liquid interface and is immiscible in the phase with optimal wetting properties. It is also interesting to note that the range of c_i for DAC spans a factor of 4, while the ranges of natural gas and coal span a factor of 6, implying that the parameter space for optimization is wider for the more concentrated gas systems.

(2) Increasing the liquid-phase mass transfer coefficient, k_L leads to enhanced CO_2 capture. The range of k_L for typical solvents having viscosities on the order of hundreds μPa s is 0.05–0.35 mm s^{-1}. For solvents such as ionic liquids with viscosities on the order of 10 000 μPa s, the range of k_L is significantly reduced by an order of magnitude, ranging from 0.001 to 0.009 mm s^{-1}. The porosity of the packing material, ε, also impacts k, ranging from 0.05 mm s^{-1} with $\varepsilon = 0.95$ up to 0.15 mm s^{-1} with $\varepsilon = 0.6$ and $L = 0.001$ m s^{-1}. With a high L of 0.01 m s^{-1} and the same porosity range, k_L ranges from 0.35 mm s^{-1} on the high end down to 0.05 mm s^{-1} at the low end. There is likely an optimized porosity of a given packing material. A lower porosity may result in less solvent-coated packing, potentially leading to a higher k_L, but minimizing porosity is practically limited because too low of a porosity inherently leads to the solvent exiting the column without interacting with CO_2. An additional opportunity for optimization exists with L. Increasing L results in an enhanced k_L, but with this increase comes an additional energy cost from solvent pumping. For solvents with the optimal viscosity (*i.e.*, 100 μPa s), k_L has the potential to vary over a factor of 7.

(3) Increasing the chemical reaction rate constant, k leads to enhanced CO_2 capture. In the case of a fast pseudo-first-order reaction, the CO_2 flux is directly proportional to $\sqrt{k}$. Spanning traditional solvents such as MEA solvents and comparing these to an unobtainium solvent, with kinetics on the order of carbonic anhydrase, leads to a potential flux increase by a factor of 100. The rate constant also plays a role when the full film model is used to calculate E since this is dependent upon $\sqrt{M}$, which in turn is directly proportional to $\sqrt{k}$. Therefore, as $\sqrt{k}$ increases, $\sqrt{M}$ increases, which leads to an increase in E, as shown in eqn (12) and Fig. 1. From Fig. 8, it can be seen that over a k range of 10^8 to 10^9 cm^3 mol^{-1} s^{-1}, $\sqrt{M}$ ranges from 2×10^4 to 4×10^4, while over a k range of 10^{10} to 10^{11} cm^3 mol^{-1} s^{-1}, the range of $\sqrt{M}$ is slightly broader, from 1×10^5 to 4×10^5. Hence, as k increases, its impact on $\sqrt{M}$ becomes greater. It is important to note that the highest $\sqrt{M}$ estimates that lead to higher E values require k_L to be less than 0.01 mm s^{-1}, as these are the conditions required for kinetics to dominate. If k_L is too large, there will not be sufficient CO_2 concentration to keep up with the chemical reaction taking place at the interface of the liquid film and bulk phase of the liquid, *i.e.*, the system becomes equilibrium-controlled rather than kinetically-controlled. Considering the range of E_i values in Fig. 6 and estimating E using these values along with $\sqrt{M}$ from Fig. 1 shows that $\sqrt{M} \approx E$ is a reasonable assumption for the case of DAC. Hence, for the full film model, solvents with a high rate constant have the potential to increase the flux by a factor of 4. In the cases of flue gas from natural gas and coal, increasing $\sqrt{M}$ leads to an increase in E, but this relationship is not as direct at a lower E_i, as shown in Fig. 1.

Table 13 Potential impact of solvent modification on CO_2 flux

	Film 3 J	Full Film J
c_i [mol cm^{-3}]		
DAC	4×	
Natural gas and coal	6×	
k [cm^3 mol^{-1} s^{-1}]		
DAC	100×	4×
Natural gas and coal	100×	2–4×[a]
k_L [mm s^{-1}]	7×	

[a] Depending on E_i from Fig. 6.

Table 13 shows the relative impact optimal solvent properties and absorption process parameters have on the CO_2 flux across the gas–liquid interface. In the case of c_i and k_L, there is no distinction in the impact between conditions of fast pseudo-first-order reaction and the full film model. It appears at first glance that k_L has a greater impact than c_i; however, since a high k_L also results in a potential depletion of CO_2 at the gas–liquid interface, it is important to consider the impact an increase in k_L would have on k. This is especially crucial since the rate constant has the greatest potential for increasing flux, in particular for the fast pseudo-first-order reaction cases. For conditions requiring the use of the full film model, it is interesting to note that increasing k has a greater impact on DAC than natural gas and coal flue gas applications. The current study provides guidance for future work to improve solvent and absorption process properties for carbon capture, suggesting that the greatest impact could be made by increasing the rate constant under the conditions of a fast pseudo-first-order reaction for systems with moderate k_L.

Acknowledgements

The authors thank Antonio Baclig, Geoffrey Holmes, and Niall MacDowell for their careful review and comments on the manuscript in its early stages.

References

1 Energy Technology Perspective, Pathways to a Clean Energy System Energy Information Agency, 2012.

Published on 25 February 2014. Downloaded by Stanford University on 19/05/2014 02:23:01.

2 Global carbon-dioxide emissions increase by 1.0 Gt in 2011 to record high, http://www.iea.org/newsroomandevents/news/2012/may/name, 27216,en.html, Accessed August 19, 2012.
3 M. R. Allen, D. J. Frame, C. Huntingford, C. D. Jones, J. A. Lowe, M. Meinshausen and N. Meinshausen, *Nature*, 2009, **458**, 1163–1166.
4 M. Meinshausen, N. Meinshausen, W. Hare, S. C. B. Raper, K. Frieler, R. Knutti, D. J. Frame and M. R. Allen, *Nature*, 2009, **458**, 1158–1162.
5 J. G. Canadell, C. Le Quere, M. R. Raupach, C. B. Field, E. T. Buitenhuis, P. Ciais, T. J. Conway, N. P. Gillett, R. Houghton and G. Marland, *Proc. Natl. Acad. Sci. U. S. A.*, 2007, **104**, 18866–18870.
6 *CO_2 Emissions From Fuel Combustion Highlights 2011 Edition*, International Energy Agency, Paris, 2011.
7 BP Energy Outlook 2030, Statistical Review, BP, London, 2011.
8 S. Pacala and R. Socolow, *Science*, 2004, **305**, 968–972.
9 J. C. Creyts, C. Board, *Reducing US Greenhouse Gas Emissions: How Much at what Cost?*, McKinsey and Company, 2007.
10 M. Mikkelsen, M. Jorgensen and F. C. Krebs, *Energy Environ. Sci.*, 2010, **3**, 43–81.
11 R. Socolow, M. Desmond, R. Aines, J. Blackstock, O. Bolland, T. Kaarsberg, N. Lewis, M. Mazzotti, A. Pfeffer, K. Sawyer, J. Siirola, B. Smit and J. Wilcox, A Technology Assessment for the APS Panel on Public Affairs, American Physical Society, June 1, 2011.
12 J. Wilcox, *Carbon Capture*, Springer, 2012.
13 X. Wang, L. Zhi and K. Mullen, *Nano Lett.*, 2007, **8**, 323–327.
14 S. Verhelst and T. Wallner, *Prog. Energy Combust. Sci.*, 2009, **35**, 490–527.
15 C. White, R. Steeper and A. Lutz, *Int. J. Hydrogen Energy*, 2006, **31**, 1292–1305.
16 A. Lewis, D. Kershner, S. Paglieri, M. Slepicka and J. Way, *J. Membr. Sci.*, 2013, **437**, 257–264.
17 K. House, A. C. Baclig, M. Ranjan, E. A. van Nierop, J. Wilcox and H. J. Herzog, *Proc. Natl. Acad. Sci. U. S. A.*, 2011, **108**, 20428–20433.
18 W. G. Whitman, *Chem. Metall. Eng.*, 1923, **29**, 146–148.
19 J. Seader, *Separation Process Principles*, John Wiley & Sons, 2006.
20 E. L. Cussler, *Diffusion: mass transfer in fluid systems*, Cambridge university press, 1997.
21 P. Dankwerts, *Gas–liquid Reactions*, McGraw-Hill, 1970.
22 W. L. McCabe, J. C. Smith and P. Harriott, *Unit operations of chemical engineering*, McGraw-Hill Book Company, New York, 1956.
23 G. Holmes and D. W. Keith, *Philos. Trans. R. Soc., A*, 2012, **370**, 4380–4403.
24 M. Mazzotti, R. Baciocchi, M. J. Desmond and R. H. Socolow, *Clim. Change*, 2013, 1–17.
25 K. Onda, H. Takeuchi and Y. Okumoto, *J. Chem. Eng. Jpn.*, 1968, **1**, 56–62.
26 J. Fair and J. Bravo, *Chem. Eng. Prog.*, 1990, **86**, 19–29.
27 G. Wang, X. Yuan and K. Yu, *Ind. Eng. Chem. Res.*, 2005, **44**, 8715–8729.
28 K. Onda, E. Sada and H. Takeuchi, *J. Chem. Eng. Jpn.*, 1968, **1**, 62–66.
29 P. Gandhidasan, *Ind. Eng. Chem. Res.*, 2003, **42**, 3420–3425.
30 D. W. van Krevelen and P. J. Hoftijzer, *Chimie et Industrie*, Brussels, 1948.
31 N. Razi, O. Bolland and H. Svendsen, *Int. J. Greenhouse Gas Control*, 2012, **9**, 193–219.
32 E. W. Lemmon, in *Thermophysical Properties of Air*, ed. D. Lide, CRC Press, Boca Raton, 92nd edn., 2011–2012.
33 J. T. Cullinane, *Thermodynamics and Kinetics of Aqueous Piperazine with Potassium Carbonate for Carbon Dioxide Absorption*, Doctoral Thesis, University of Texas at Austin, 2005.
34 A. Melinder, *Thermophysical Properties of Aqueous Solutions Used as Secondary Working Fluids*, Doctoral Thesis, Royal Institute of Technology, KTH, 2007.
35 D. Sanyal, N. Vasishtha and D. N. Saraf, *Ind. Eng. Chem. Res.*, 1988, **27**, 2149–2156.
36 H. Tokuda, S. Tsuzuki, M. A. B. H. Susan, K. Hayamizu and M. Watanabe, *J. Phys. Chem. B*, 2006, **110**, 19593–19600.
37 J. G. Huddleston, A. E. Visser, W. M. Reichert, H. D. Willauer, G. A. Broker and R. D. Rogers, *Green Chem.*, 2001, **3**, 156–164.
38 C. Guerrero-Sanchez, T. Lara-Ceniceros, E. Jimenez-Regalado, M. Raşa and U. S. Schubert, *Adv. Mater.*, 2007, **19**, 1740–1747.
39 S. V. Dzyuba and R. A. Bartsch, *ChemPhysChem*, 2002, **3**, 161–166.
40 T. Amundsen, L. Oi and D. Eimer, *J. Chem. Eng. Data*, 2009, **54**, 3096–3100.
41 B. P. Mandal, M. Kundu and S. S. Bandyopadhyay, *J. Chem. Eng. Data*, 2003, **48**, 703–707.
42 B. P. Mandal, M. Kundu and S. S. Bandyopadhyay, *J. Chem. Eng. Data*, 2005, **50**, 352–358.
43 B. P. Mandal, M. Kundu, N. U. Padhiyar and S. S. Bandyopadhyay, *J. Chem. Eng. Data*, 2004, **49**, 264–270.
44 N. Razi, O. Bolland and H. Svendsen, *Int. J. Greenhouse Gas Control*, 2012, **9**, 193–219.
45 E. B. Rinker, D. W. Oelschlager, A. T. Colussi, K. R. Henry and O. C. Sandall, *J. Chem. Eng. Data*, 1994, **39**, 392–395.
46 T. T. Teng, Y. Maham, L. G. Hepler and A. E. Mather, *J. Chem. Eng. Data*, 1994, **39**, 290–293.
47 A. Muhammad, M. I. A. Mutalib, T. Murugesan and A. Shafeeq, *J. Chem. Eng. Data*, 2008, **53**, 2217–2221.
48 E. Alvarez, R. Rendo, B. Sanjurjo, M. Sanchez-Vilas and J. M. Navaza, *J. Chem. Eng. Data*, 1998, **43**, 1027–1029.
49 P. W. Derks, K. J. Hogendoorn and G. F. Versteeg, *J. Chem. Eng. Data*, 2005, **50**, 1947–1950.
50 D. W. Savage, G. Astarita and S. Joshi, *Chem. Eng. Sci.*, 1980, **35**, 1513–1522.
51 J. T. Cullinane and G. T. Rochelle, *Chem. Eng. Sci.*, 2004, **59**, 3619–3630.
52 H. Herzog, *Assessing the Feasibility of Capturing CO_2 from the Air*, Massachusetts Institute of Technology, 2003.
53 D. Morgan, L. Ferguson and P. Scovazzo, *Ind. Eng. Chem. Res.*, 2005, **44**, 4815–4823.
54 H. Hikita, S. Asai, H. Ishikawa and M. Honda, *Chem. Eng. J.*, 1977, **13**, 7–12.

 This journal is © The Royal Society of Chemistry 2014

Published on 25 February 2014. Downloaded by Stanford University on 19/05/2014 02:23:01.

55 M. Caplow, *J. Am. Chem. Soc.*, 1968, **90**, 6795–6803.
56 J. E. Crooks and J. P. Donnellan, *J. Chem. Soc., Perkin Trans. 2*, 1989, 331–333.
57 R. A. Tomcej and F. D. Otto, *AIChE J.*, 1989, **35**, 861–864.
58 F. Camacho, S. Sanchez, R. Pacheco, M. D. La Rubia and A. Sanchez, *Int. J. Chem. Kinet.*, 2009, **41**, 204–214.
59 S. Bishnoi and G. T. Rochelle, *Chem. Eng. Sci.*, 2000, **55**, 5531–5543.
60 R. Billet and M. Schultes, *Chem. Eng. Technol.*, 1993, **16**, 1–9.
61 V. Engel, J. Stichlmeir and W. Geipel, *Chem. Eng. Technol.*, 2001, **24**, 459–462.
62 Z. Olujic, M. Behrens, L. Colli and A. Paglianti, *Chem. Biochem. Eng. Q.*, 2004, **18**, 89–96.
63 J. A. Rocha, J. L. Bravo and R. James, *Ind. Eng. Chem. Res.*, 1996, **35**, 1660–1667.
64 S. Shetty and R. L. Cerro, *Ind. Eng. Chem. Res.*, 1997, **36**, 771–783.
65 P. Suess and L. Spiegel, *Chemical Engineering and Processing: Process Intensification*, 1992, **31**, 119–124.
66 L. Del Carlo, Z. Olujic and A. Paglianti, *Ind. Eng. Chem. Res.*, 2006, **45**, 7967–7976.
67 J. B. Tepe and B. F. Dodge, *Trans. Am. Inst. Chem. Eng.*, 1943, **39**, 255–276.
68 N. A. Spector and B. F. Dodge, *Trans. Am. Inst. Chem. Eng.*, 1946, **42**, 827–848.
69 C. Wilke and P. Chang, *AIChE J.*, 1955, **1**, 264–270.